Laboratory Studies of Langmuir Circulations

ALAN J. FALLER

Institute for Physical Science and Technology, University of Maryland, College Park 20742

RANDALL W. CARTWRIGHT[1]

Department of Meteorology, University of Maryland, College Park 20742

(Manuscript received 21 May 1982, in final form 27 September 1982)

ABSTRACT

Laboratory studies of the interaction of crossed waves (on water) and a wind-induced shear are found to be in quite general agreement with the Craik-Leibovich (CL) theory of Langmuir circulation (LC's). The LC's develop rapidly, convect turbulent fluid to the bottom, and significantly modify the surface current by a vertical exchange of momentum. Reversal of the wind direction relative to the waves is found to reverse the sense of rotation of the LC's, a specific prediction of the CL theory.

1. Introduction

In an earlier report (Faller, 1978, hereafter F) preliminary laboratory experiments were described which presented experimental evidence essentially in agreement with the earlier Craik-Leibovich theory of Langmuir circulations (LC's). This short paper presents additional confirming evidence from variants of the earlier experiments.

The Craik-Leibovich theories may be divided into two categories that are here referred to as the CL I and the CL II theories (models, mechanisms). In CL I a pattern of crossed irrotational waves, a simplified representation of the three-dimensional ocean surface, interacts with a vertical shear caused by the wind stress. In essence, the finite-amplitude waves twist the vortex lines of the shear flow into a series of alternating helical rolls, the Langmuir circulations (LC's), having an across-wind wavelength determined by the wave pattern. This process is described in Craik and Leibovich (1976), Leibovich (1977a) and Leibovich and Radhakrishnan (1977). In Craik (1977) an instability mechanism was recognized in which the average Stokes drift of a progressive, but otherwise random, wave field interacts with the wind-driven shear flow. This mechanism has been elaborated in Leibovich (1977b), Paolucci (1979) and Leibovich and Paolucci (1980a, b, 1981) and is here referred to as the CL II theory.

Because of the complexity of the ocean surface under windy conditions it seems unlikely that the CL mechanisms of wave and shear-flow interactions will ever be unambiguously verified by observations in the field. Despite the apparent success of the theory, one can imagine that other processes, for example variations of wind stress over the waves or spatial variations of turbulence associated with the waves, may also lead to elongated patterns of vorticity by interactions not yet analyzed or imagined. Thus one should retain a certain small degree of skepticism until other possibilities have been exhausted. For the same reasons, in the experiments of Faller and Caponi (1978, hereafter FC), where wind-generated waves caused the LCs, it was not possible to clearly distinguish between the CL I and the CL II mechanisms or other possibilities. One might be inclined to attribute those LC's to the CL II mechanism, but the waves in those experiments (see photographs in FC) clearly showed patterns with quasi-hexagonal and/or crossed-wave structure.

The author's reservations with respect to existing theories have been whetted by the work of Mobley (1977) who generated a three-dimensional numerical model of crossed waves with variable height of the free surface and with a stress-induced shear flow. The model accurately reproduced the shape of finite-amplitude waves (in agreement with third-order Stokes theory), and the crossed waves reproduced the theoretical pattern of Stokes drift (Leibovich, 1977a) as shown from the Lagrangian trajectories of surface markers. When shear flow was added, however, the model failed to produce LC's under conditions where they should have occurred according to the CL I theory.

One is inclined to dismiss these negative results as being due to numerical error of some sort, or, pos-

[1] Present affiliation: Naval Research Laboratory, Code 4310, Washington, DC 20375.

sibly, due to incorrect surface-stress conditions. Indeed, some difficulties may have arisen from poor resolution of the cells, and the correct method of applying a fully nonlinear stress in finite-difference form over a moving three-dimensional surface was not clear. Instead, a linearized, constant horizontal stress was applied, one that appeared to correspond to that of the CL theories. But one cannot argue the merits or shortcomings of the numerical model in this short paper, and Mobley's study is cited here simply as motivation for further three-dimensional numerical simulations and for further laboratory tests of the reality of the CL theories.

2. Experimental apparatus

Fig. 1 illustrates the basic laboratory apparatus, which is described in more detail in F and in FC. In brief, crossed waves are generated by a vertically oscillating pair of wedges at the first resonant frequency, $\sigma = 10.604\ s^{-1}$. Assuming a right-hand coordinate system with x along the direction of the wave propagation and z vertically upward, distance across the tank is from $y = 0$ at the near wall to $y = Y = 88$ cm at the far wall.

The velocity potential of a crossed-wave pattern has been given by Leibovitch (1977a) as

$$\phi = 2a\sigma k^{-1}e^{kz}\cos[(k\sin\theta)y]\cos[(k\cos\theta)x - \sigma t], \quad (1)$$

where a is the amplitude of a single wave, k the (diagonal) wavenumber, θ the angle of each wave crest with respect to the y axis, $k\sin\theta$ is the apparent wavenumber along y, and $k\cos\theta$ the apparent wavenumber along x. In these experiments $\theta = \pi/4$, and it follows that $k = 2^{3/2}\pi/Y$.

At a fixed x the waves appear to be a standing wave with nodes at $y = Y/4$ and $3Y/4$, and with antinodes at $y = 0$, $Y/2$ and Y. These latter positions also locate the traces of the wave crest (and wave trough) intersections as the wave pattern moves along x. The wave height as observed on the side wall was 2.4 cm, and it follows that the amplitude of each contributing diagonal wave was 0.6 cm as in F.

In the experiments to be described, the water depth was $H = 17$ cm rather than $H = 39$ cm as in F. This reduced depth was arranged by adding a false bottom to provide a depth compatible with the cell wavelength $\lambda_c = 44$ cm, the scale forced by the wave pattern. As clearly shown in FC and in earlier experiments (Faller, 1969), with relatively large water depth (i.e. compared to the scale at which cells are forced), the energy of small cells cascades to larger scales, and the eventually-dominant cell size has an across-wind wavelength $\lambda_c \approx 2.5H$. The use of $H = 17$ cm thus was intended to minimize the exchange of energy between that scale forced by the waves, according to the CL I theory, and other possible scales.

For prograde winds, as in the earlier experiments and as in Section 3, air was drawn into the tunnel in front of the wavemaker (see Fig. 1) by a fan in a tower at the extreme right-hand end of the tank (FC). Wind speeds ranged from 100 to 400 cm s^{-1}. For retrograde winds (Section 4), i.e., opposed to the waves, the fan was reversed. Unfortunately, the retrograde wind had poor entrance conditions and could not be made as uniform across the tank as was the prograde wind.

It was reported in F that with waves (but no wind) or with light wind (but no crossed waves) plastic floats remained more or less uniformly distributed across the tank. With both light wind and crossed waves,

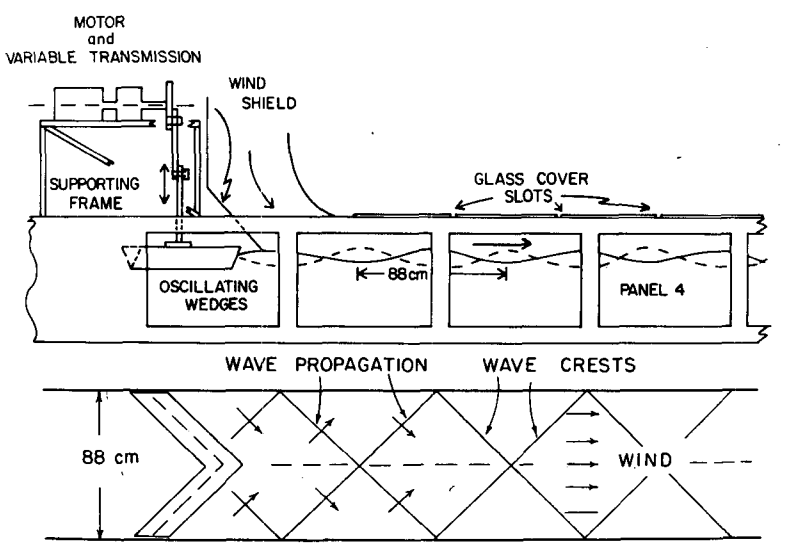

FIG. 1. Essential features of the wind and wave tank and the regular pattern of waves produced by the double-wedge wave generator. The illustrated wave amplitude is very much exaggerated over reality. (From Faller, 1978.)

however, the floats rapidly lined up along the nodal lines at $y = Y/4$ and $3Y/4$, in agreement with the CL I theory. The transient rate of development of the LCs was determined from a series of experiments with measurements of float trajectories a short time after onset of the wind (waves being already present) or after onset of the waves (the wind being already present).

By means of dye spread on the bottom, in that case at $z = -39$ cm, it was shown that the cells rapidly convected turbulent surface water to the bottom where the dye gradually became organized in bands beneath the antinodes and was then convected upward (see Fig. 2).

The prograde wind experiments of Section 3 used the same plastic floats, 2.5 cm long and 1.25 cm in diameter, as in F. It has been found, however, as discussed in Section 4, that these tracers may have some peculiar action in the complex water motion and may not truly indicate the surface water velocities. For the experiments of Section 4, the plastic floats were replaced by ordinary ¼ inch diameter paper dots. But, whereas the plastic floats had the advantage of being essentially uninfluenced by surface film, the paper dots required a completely film-free surface.

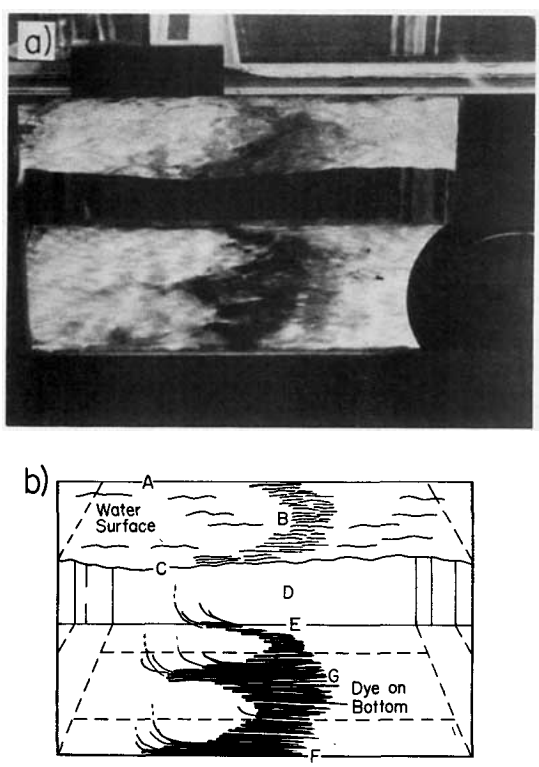

FIG. 2. (a) An oblique photograph covering side panel 4 (Fig. 1) to illustrate the pattern of dye at the tank bottom in W5 (Faller, 1978). (b) A schematic diagram to clarify the photograph. A, the upper edge of glass panel 4; B, the pattern of bottom dye as seen refracted through the wavy water surface; C, the profile of surface waves along the glass panel; D, a dark background looking through the tank; E and F, the far and near edges of the tank bottom; G, the pattern of bottom dye with a superimposed complex light pattern from light passing through the wavy free surface.

3. Growth-rate experiments

a. General conditions and procedures

The experiments reported in F produced cells with approximately an exponential growth rate described by

$$V(t) = V(\infty)\exp(-t/T), \tag{2}$$

where $V(t)$ was the maximum surface velocity of the cells at time t, $V(\infty)$ the value approached at large t, and T the time constant. For the wind speed $\bar{w} = 173$ cm s^{-1} the values $V(\infty) = 0.65$ cm s^{-1} and $T = 12$ s were found. The cells, each having an across-wind width of 22 cm (wavelength $\lambda_c = 44$ cm), carried turbulent surface water to a depth of 39 cm in about 90 s, thus indicating a vertically-averaged downwelling speed of 0.43 cm s^{-1} for the initial turbulent pulses.

The following experiments were among several performed to develop an alternate and perhaps more efficient method of determining $V(\infty)$ and T for a variety of experimental conditions. The analysis of data proved to be very time consuming, however, and only these two cases have been analyzed.

The experimental conditions were nearly identical to those in F except that different wind speeds were used and the depth of water was reduced from 39 to 17 cm by the addition of a false bottom to the tank. The two experiments had wind speeds, measured 5 cm above the water surface, of $\bar{w}_4 = 139$ cm s^{-1} (case W4) and $\bar{w}_7 = 232$ cm s^{-1} (case W7). The single experimental condition used in F has $\bar{w}_5 = 173$ cm s^{-1} and that case is referred to as W5. From an empirical relation in Schlichting (1960) for wall stresses in a channel, the wind stress on the water (ignoring the effects of waves and water motion) is assumed to be given approximately by

$$\tau/\rho = 0.0103u^{1.75}, \tag{3}$$

and numerical values are given in Table 1.

To begin an experiment, with the wind blowing (but with no crossed waves) three sets of plastic floats (about 60 in each set) were dumped into the tank through a glass-cover slot (Fig. 1) at 30 s intervals. (These slots were normally taped over, but were uncovered for the introduction of dye crystals and tracers.) In this process the wind distributed the floats over the field of view of the cine camera and also blew away the surface film to the far (right-hand) end of the tank. Since the floats were inserted close to the wind intake, the wind-generated waves were small and did not lead to noticeable banding of the floats before onset of the crossed waves (Figs. 3 and 4). The 16 mm camera, operated at 12.85 frames per second, was mounted 2 m above the water surface, and its

TABLE 1. Experimental conditions for W4 and W7 and the fitted values of t_0, T, $V_{S2}(\infty)$, $V_{S4}(\infty)$ and $U_{C2}(\infty)$ for the curves of Figs. 5 and 6. The initial values of the average wind-driven flow $U_0(0)$ in the surface layer before the onset of the crossed waves are also given. Corresponding data for W5, the similar case discussed in Faller (1978), are given for comparison where available.

Case	H	Wind	τ/ρ	t_0	T	$V_{S2}(\infty)$	$V_{S4}(\infty)$	$U_{C2}(\infty)$	$U_0(0)$
				All numerical values are in cgs units.					
W4	17	139	58	−2.4	2.6	0.43	−0.21	0.17	1.70
W5	39	173	85	—	12	0.65	—	—	—
W7	17	232	142	−0.2	15	1.68	0	−1.61	3.96

field of view covered that portion of the tank with glass side panels 3 and 4 (Fig. 1).

The waves and cine camera were turned on simultaneously. Because the tracers were spread out along x and because the growth of the cells at any particular location would depend upon the time elapsed after passage of the first wave, the speed of propagation of the wave energy along x had to be accounted for in order to combine data from tracers at different x. Time relative to passage of the wave front was determined from

$$t = (t' - t_r) - c_{gx}x, \tag{4}$$

where t' is real time, t_r a reference time, and c_{gx} is the rate of propagation of wave energy along x.

Denoting c as the diagonal phase speed of a wave, c_g as the diagonal group speed, and c_x as the apparent phase speed along the wall of the tank, it follows that $c_x = 2^{1/2}c$ and $c_{gx} = 2^{-1/2}c_g$. In deep water (as in F) one would find $c_{gx} = c_x/4$, but because of the finite depth (H = 17 cm) it is found from theory that $c_{gx} = c_x/3.3$.

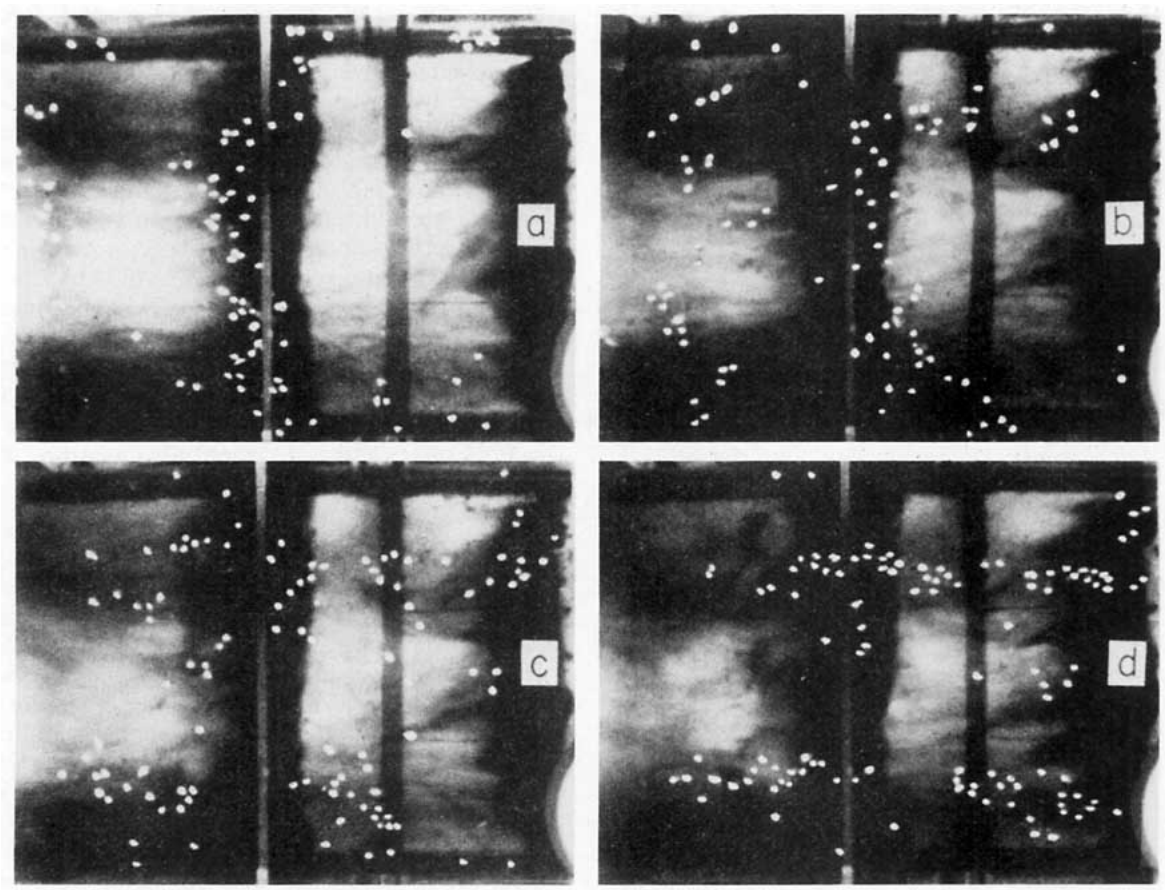

FIG. 3. A sequence of surface float positions for W4. These photographs are centered 225 cm from the wave generator and include panel 3 and half of panel 4 (Fig. 1). Float positions have been enhanced and enlarged by opaque white dots. (a) t = 0, (b) t = 12.5 s, (c) t = 24.9 s, (d) t = 37.4 s. In Figs. 3 and 4 a one-to-one correspondence of tracers in successive photos is not possible. Tracers are sometimes hidden, shaded or indistinguishable from the background for various reasons.

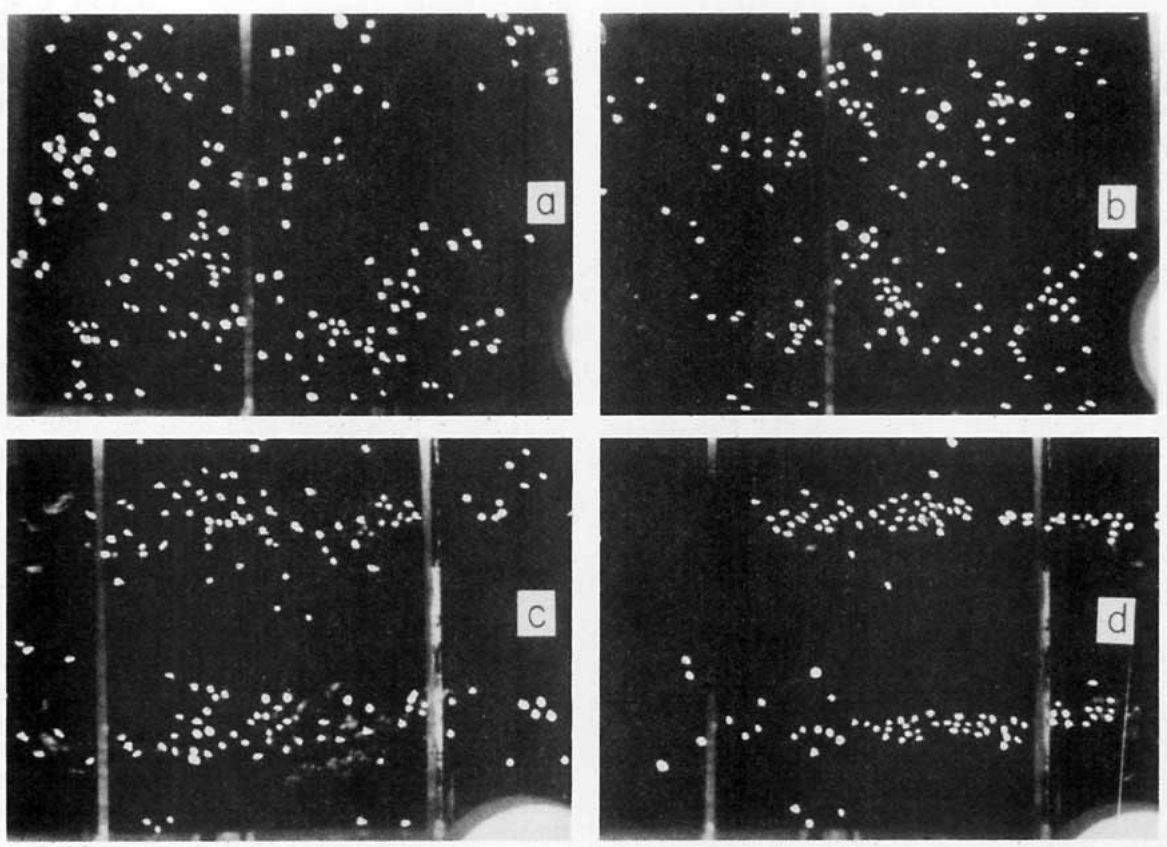

FIG. 4. As in Fig. 3 but for W7 with photos at half the interval of Fig. 3.
(a) $t = 0$, (b) $t = 6.2$ s, (c) $t = 12.5$ s, (d) $t = 18.7$ s.

For the desired regular pattern of crossed waves, the geometry of the tank requires a fixed diagonal wavelength $K = 88/2^{1/2} = 62.2$ cm. The corresponding theoretically required resonant wave frequency is $\sigma_{th} = 9.635$ s^{-1}. The measured resonant frequency, that which appeared to give the best wave pattern, was $\sigma = 10.604$ s^{-1}, larger than σ_{th} by about 10%. This higher frequency probably was required to compensate for the surface flow due to the wind, a drift of a few centimeters per second, and other factors not included in the theory. Accordingly, the group speed along x was assumed to be 10% larger than the theoretical value, and the value used in (4) was $c_{gx} = 45.0$ cm s^{-1}, a speed in good agreement with the observed rate of propagation of wave energy.

b. Data analysis

Cine films of the tracer motions were projected onto the table of a coordinate digital converter, and the tracer positions at intervals of 8 frames (0.623 s) were recorded on punched paper tape for computer analysis of the velocities. The precision of the recorder was ±0.003 cm and the accuracy of location of a tracer was ±0.013 cm for either the x or y positions. The corresponding rms error of the component speeds over the 8-frame time interval was ±0.03 cm s^{-1}.

Systematic errors due to optical distortions were accounted for in the data analysis by relating the observed coordinates of a point to the precisely known coordinates of an array of fixed points. Another type of bias was present because of the small difference between the wave frequency, $\sigma = 10.604$ s^{-1}, and the frequency of analysis of the cine film, $\sigma_f = 10.092$ s^{-1}. This introduced a type of aliasing of the wave velocities. With the given frequencies and wave amplitude it is calculated that the maximum contribution from the waves to an 8-frame average velocity would be ±0.44 cm s^{-1} and the rms contribution would be ±0.22 cm s^{-1}. These contributions to individual speeds are substantial, but the subsequent data analysis averaged the contributions of some 200 tracers more or less randomly spaced in x and y and over a 1 s interval, so the wave contribution was smoothed out.

The positions and velocity components for all tracers were ordered in time relative to the time of arrival of the waves using (4). The tracers then were grouped into overlapping 1 s intervals centered at every 0.5 s. There were ~200 tracers in each group. Thus the velocities in each 1 s group were from tracers spread

out along x, but all were within a 1 s interval relative to the onset of waves.

All velocities in each interval were subjected to a least-squares Fourier analysis in y to determine the coefficients in the equations

$$\hat{v}_i(y) = V_{0,i} + \sum_{n=1}^{N} V_{Cn,i} \cos\left(\frac{2\pi ny}{88}\right) + V_{Sn,i} \sin\left(\frac{2\pi ny}{88}\right), \quad (5)$$

$$\hat{u}_i(y) = U_{0,i} + \sum_{n=1}^{N} U_{Cn,i} \cos\left(\frac{2\pi ny}{88}\right) + U_{Sn,i} \sin\left(\frac{2\pi ny}{88}\right), \quad (6)$$

where $\hat{v}_i(y)$ and $\hat{u}_i(y)$ are estimates of $v_i(y)$ and $u_i(y)$, and where the subscript i indicates one of the 1 s time intervals. The regression coefficient $V_{Cn,i}$, for example, refers to the nth cosine coefficient of $v(y)$ for the ith time step. The sines and cosines would be independent variates if the data points were equally spaced across the tank, but since this was not the case, the values of the coefficients depend to some extent upon N, the number of components used in (5) and (6).

In trial calculations the coefficients of the principal components were found to be essentially the same for $N = 4$, 6 and 8. The values presented below are from calculations with $N = 6$ in which only the V_{Sn} and the U_{Cn} were determined, since for regular cells we expect only sine components in $v(y)$ and only cosine components in $u(y)$.

c. *Experimental results*

Fig. 3 shows a sequence of tracer positions at 12.46 s intervals (160 frames) for W4, and Fig. 4 shows a similar sequence for W7 at 6.23 s intervals (80 frames). The convergence of tracers into lines at the nodes of the wave pattern, $y = Y/4$ and $3Y/4$, is obvious. The evolutions of the Fourier components V_{S2}, V_{S4}, U_{C2} and U_{C4} for these two cases are shown in Figs. 5 and 6. Data analysis was terminated at about 11 s because, as may be seen in Figs. 3 and 4, by 12 s the tracers were becoming too concentrated to be representative of all y.

Fig. 7 illustrates and interprets the meanings of some of the principal Fourier components to be expected from regular cells. While V_{S2} needs no further comment, some physical explanation of V_{S4} and U_{C2} is instructive.

It is well known from observations (e.g., Scott *et al.*, 1969) and now from numerical calculations (Leibovich and Radhakrishnan, 1977) that the downwelling in LC's is more concentrated with higher speeds than the upwelling. A qualitative explanation of this asymmetry has been offered by Csanady (personal communication) in terms of the hydrodynamic concept of image vortices as in Fig. 7a. The image vortices represent the effect of the free surface which limits the vertical extent of the real vortices. In vortex theory, each vortex is advected by the extended circulations of all other vortices, and in the present case the net effect of the image vortices is to cause the real vortices to crowd together in pairs toward the surface convergence lines. The resultant asymmetry gives a negative value of V_{S4} as in Fig. 7b. This is clearly seen to occur in W4 (Fig. 5) but is absent in W7 (Fig. 6).

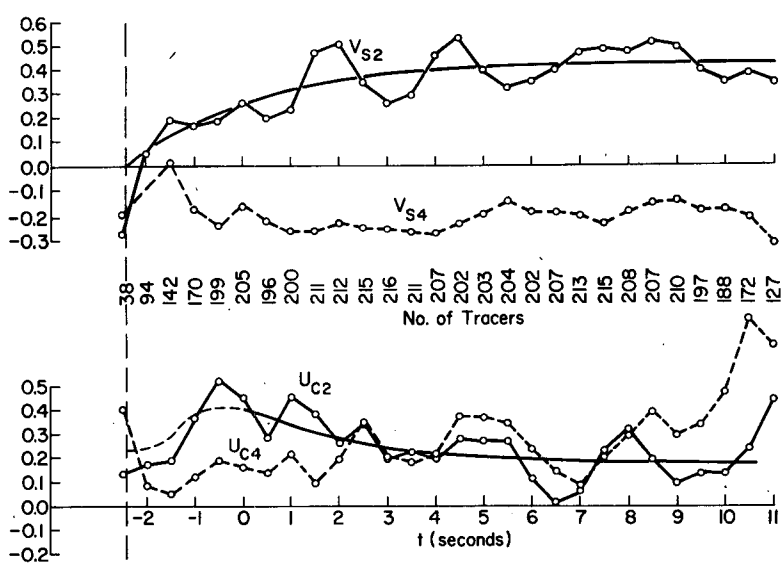

FIG. 5. Plots of the Fourier components of V_{S2}, V_{S4}, U_{C2} and U_{C4} versus time for W4. The continuous lines are the curves of best fit for V_{S2} and U_{C2}. The vertical dashed line shows the virtual time of onset of the waves for best fit, $t_0 = -2.4$ s.

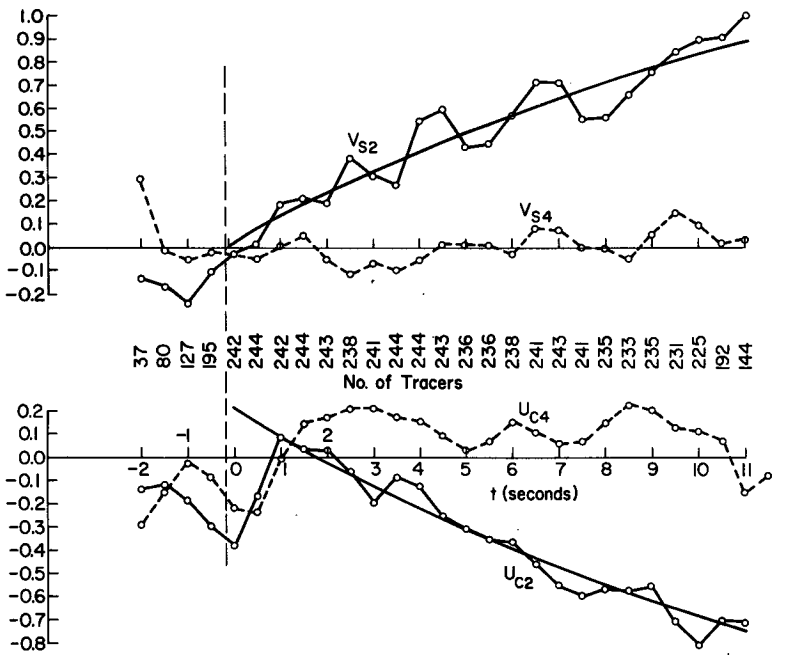

FIG. 6. Plots of the Fourier components of V_{S2}, V_{S4}, U_{C2} and U_{C4} versus time as in Fig. 5 but for W7.

U_{C2} arises from two sources that oppose each other in sign, as illustrated in Fig. 7c. The Stokes drift of the forced waves has been given by Leibovich (1977a) for deep-water waves as

$$u_s = 2\sigma a^2 k e^{kz} \cos\theta\{1 + \cos^2\theta \cos[2(k \sin\theta)y]\}, \quad (7)$$

where θ is the absolute value of the angle of each wave crest with the y axis; and in the present case $\theta = \pi/4$. To determine U_{C2}(s) (Stokes) we have used (7), thus ignoring the small effect of a finite depth. Taking into account the 2.5 cm depth of the tracers, we found $U_{C2}(s) \approx 0.23$ cm s^{-1}.

The second source of U_{C2} is a finite-amplitude effect of the LC's. Surface water drifting toward the convergence line accumulates momentum from the effect of the wind stress. The net result, U_{C2}(c) (cells), depends upon many factors involved in the overall surface momentum balance. Apparently in W4 U_{C2}(s) dominated U_{C2}(c) (Fig. 5) and in W7 the reverse was true (Fig. 6) because of the much stronger cells. No simple interpretation of U_{C4} can be given, but in both cases it was positive and thus contributed to maxima in u along the convergence lines.

The data points for $V_{S2,i}$ in Figs. 5 and 6 were fit (see Appendix A) by exponentials of the form

$$\hat{V}_i = V_{S2}(\infty)\left[1 - \exp\left(-\frac{t_i - t_0}{T}\right)\right],$$

where $\hat{V}_i$ is an estimate of $V_{S2,i}$, $V_{S2}(\infty)$ is the long-time equilibrium value, T the time constant and t_0 the starting time. The values found for $V_{S2}(\infty)$, T and t_0 are listed in Table 1 and the fitted curves are drawn in Figs. 5 and 6.

The curve fitted to U_{C2} in Fig. 6 used the values of T and t_0 found for V_{S2}. Then $U_{C2}(t_0)$ and $U_{C2}(\infty)$ were found by the usual least-squares method. The resultant curve fits the data well and intersects the ordinate $t = t_0$ at $U_{C2}(t_0) = 0.23$, precisely the value calculated for U_{C2}(s). On the other hand in W4 (Fig. 5) it appears that the cells never became sufficiently vigorous for U_{C2}(c) to overcome U_{C2}(s), and prior to $t = 2$ U_{C2} is characterized by unexplained fluctuations.

Table 1 and Fig. 5 show that in W4 we had $V_{S4} \approx V_{S2}/2$. It is easily shown that if $V_{S4} > V_{S2}/2$ there are narrow convergence lines at $y = 0$, $Y/2$ and Y in addition to the major convergence lines at $y = Y/4$ and $3Y/4$. In Fig. 3 it may be seen that several tracers remained in the center of the tank and near the walls for a rather long time. The same apparent effect of higher modes also was found in FC where floats remained half way between the principal convergence lines for an unusually long time considering the finite wave and turbulent fluctuations that would tend to jostle them into one or the other of the neighboring major cells.

The three values of $V_{S2}(\infty)$ in Table 1 show a significant increase with τ/ρ, but no functional relation can be even suggested because of uncertainties in both variates. While the values of $V_{S2}(\infty)$ appear to be reasonably well determined for W4 and W5, that for W7 is very uncertain. In fact, in obtaining the smooth curve of Fig. 6 the value of V_{S2} at $t = 11$ s was omitted

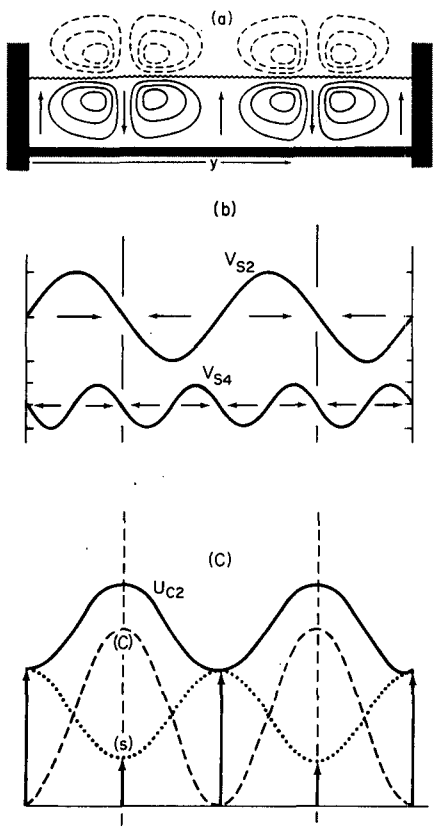

FIG. 7. The expected Fourier components of surface flow. (a) A schematic diagram of asymmetrical cells and their image vortices above the water surface. (b) The components V_{S2} and $V_{S4} \approx V_{S2}/2$, for asymmetrical cells as in (a) and as shown for W4 in Fig. 5. (c) The total U_{C2} (solid curve) as a linear sum of that due to the Stokes drift of the waves, $U_{C2}(s) > 0$ (dotted curve), and that due to the cumulative effect of the wind stress, $U_{C2}(c) < 0$ (dashed curve). In this example, as in the later stages of W7, $U_{C2}(c) > U_{C2}(s)$.

from the data. If that point is included the fitted values change from those of Table 1 to $V_{S2}(\infty) = 2.51$ cm s^{-1} and $T = 25.0$ s.

The values of T also increase with τ/ρ, a fact that clearly contradicts the simple linear model suggested in F. In that model the growth of the cells was assumed to be limited by turbulent dissipation and the time scale was given by

$$T = (2\nu_e \lambda_c^2)^{-1}, \tag{8}$$

where ν_e is a constant turbulent viscosity. Then if we assume that ν_e increases with τ/ρ, Eq. (8) shows that T should decrease with τ/ρ.

This dilemma may be rationalized if we assume that the growth of the large cells is only partially caused by the large and regular crossed waves, and that at the higher wind stresses an important source of energy comes from the wind-generated waves with an energy cascade up the spectrum from small to large LC's. If such is the case the rate of growth of V_{S2} may in fact be limited by the rate of generation of small-scale LC's and/or the rate of energy transfer from small to large scales.

With respect to the above argument, a major difference between W4 and W7 was the degree of turbulence. In W4 the wind-generated waves were small and of relatively little consequence and, from Fig. 5, V_{S2} and V_{S4} behaved in their expected way and rapidly approached equilibrium values. In W7, however, the wind-generated waves were significant, and the surface layer was obviously much more turbulent than in W4. It seems likely, therefore, that the wind-generated waves contributed significantly to the large LC's by the cascade from smaller to larger cells. Turbulence and many vigorous smaller cells may also account for the lack of a systematic $V_{S4} < 0$ as well as for the relatively slow growth rates of V_{S2} and U_{C2} in W7.

Vertical velocities were not generally observed in these experiments because the water was usually made opaque for optimum visibility of the surface tracers. In W4, however, the water was clear and potassium permanganate crystals were spread on the tank bottom to observe the deep flow patterns similar to those of Fig. 2. In Fig. 3 the somewhat irregular dye patterns in panels a, b and c are primarily due to the cumulative effect of very weak thermal convection for several minutes prior to the onset of waves. In Fig. 3d, however, several rings of dye with relatively clear centers are apparent in the left center of the photo. These signaled the arrival of downward jets impinging on the bottom and spreading the dye. Upon inspection of the cine film these pulses were first evident at about 16 s after passage of the wave front, thus indicating a vertically averaged downward speed of about 1 cm s^{-1}. These initial pulses, however, are not representative of the average overturning speeds in W4 which, judging from the other data, are probably more like 0.5 cm s^{-1}.

Fig. 8 gives the time dependence of U_0 for W4 and W7. Prior to the onset of waves the wind drifts in the 2.5 cm deep surface layer (that represented by the tracer) were about 1.70 and 3.96 cm s^{-1}, respectively. With the onset of waves U_0 first increased, apparently due to the Stokes drift of the waves. The subsequent slow decreases of U_0 undoubtedly reflected the vertical exchange of momentum associated with the growing cells which apparently continued to decrease U_0 well beyond the length of our analyzed record.

The local response of U_0 to changes in the overall momentum balance involves the redistribution of momentum throughout the entire tank and cannot be analyzed with the available data. Thus, the data of Fig. 8 suggest much longer response times than found for the growth of the cells. In addition, the initial growth of U_0 due to Stokes drift took about four wave periods (2 s), somewhat longer then one might expect.

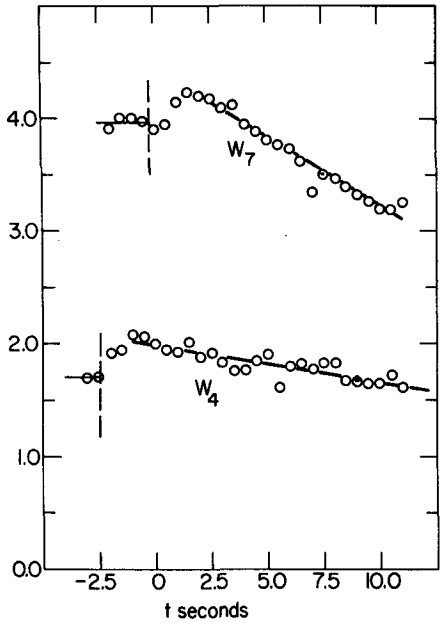

FIG. 8. Time variations of U_0, the average surface-layer flow, for W4 and W7. Horizontal lines show the approximate surface-layer flow (2.5 cm deep) due to wind stress alone. Vertical dashed lines indicate the onset of waves. Sloping lines are straight-line fits to the data after 2 s of waves.

From (7) the average Stokes drift should have been about 0.46 cm s^{-1}. This increase was not quite realized either in W4 or W7, however, apparently because by the time of 2 s the increased vertical momentum exchange due to the rapidly growing LCs had already begun.

4. Retrograde-wind experiments

The CL theories assume the waves to be irrotational, and the vorticity of the LC's is derived from the vorticity of the shear flow caused by the wind stress. In the experiments of Section 3, the basic vorticity due to the wind had the principal component $\eta = \partial u/\partial z > 0$. (The extent of other components caused by turbulence in the wind and due to the air flow over the regular wave pattern is not known.) If the wind direction is reversed to produce a basic vorticity $\eta < 0$, it follows from the CL I theory that the vorticity of the cells, in relation to the crossed-wave pattern, should also be reversed. Then the convergence lines should coincide with the antinodes, i.e., they should lie along $y = 0$, $Y/2$ and Y.

The retrograde-wind experiments were first tried using the same plastic floats as those in the experiments of Section 3, but the results were disappointing. There was an occasional tendency for the tracers to line up according to expectations, but more often they remained irregularly dispersed, or assumed a pattern like that sketched in Fig. 9a, with tracers congregating irregularly in groups on both sides of the antinodes. As they moved downwind the central tracers often merged into a sinuous line as in Fig. 9b. It was thought that these erratic patterns might be due to poor wind distribution, but efforts to more evenly distribute the air flow by means of rods and baffles did not seem to change the general response of the tracers, and so the initial retrograde-wind experiments were temporarily abandoned.

In later trial experiments, paper dots (from a 3-hole paper punch) were used as surface tracers together with the plastic floats, and the responses of the two tracers were found to be significantly different. The paper dots lined up quickly along the antinodes and then moved in straight lines. By implication it would appear that the more massive plastic floats respond to the complex of wave motions, shear and turbulence in a way that is not wholly representative of the horizontal water motions near the surface.

The retrograde-wind experiments with paper dot tracers are shown in Figs. 10 and 11. Fig. 10 is an example with both waves and wind, and shows the paper dot distribution 10 s after the waves first reached the tracers. Fig. 11 was an identical experiment except for the absence of the crossed waves.

The sequence of events leading to Fig. 10 was as follows:

1) Starting with water at rest, the wind was turned on at -330 cm s^{-1} to blow away the ever-present

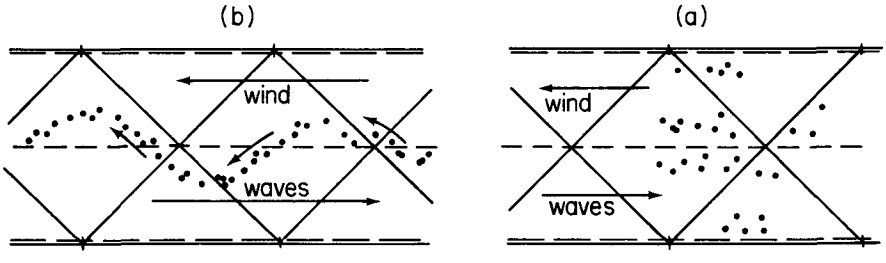

FIG. 9. Patterns of plastic floats frequently observed in the retrograde wind experiments. (a) Floats more or less in lines but apparently avoiding the traces of the wave crest (and wave trough) intersections, the dashed lines. (b) A sinuous line of floats progressing downwind. The paper dot tracers showed neither of these patterns.

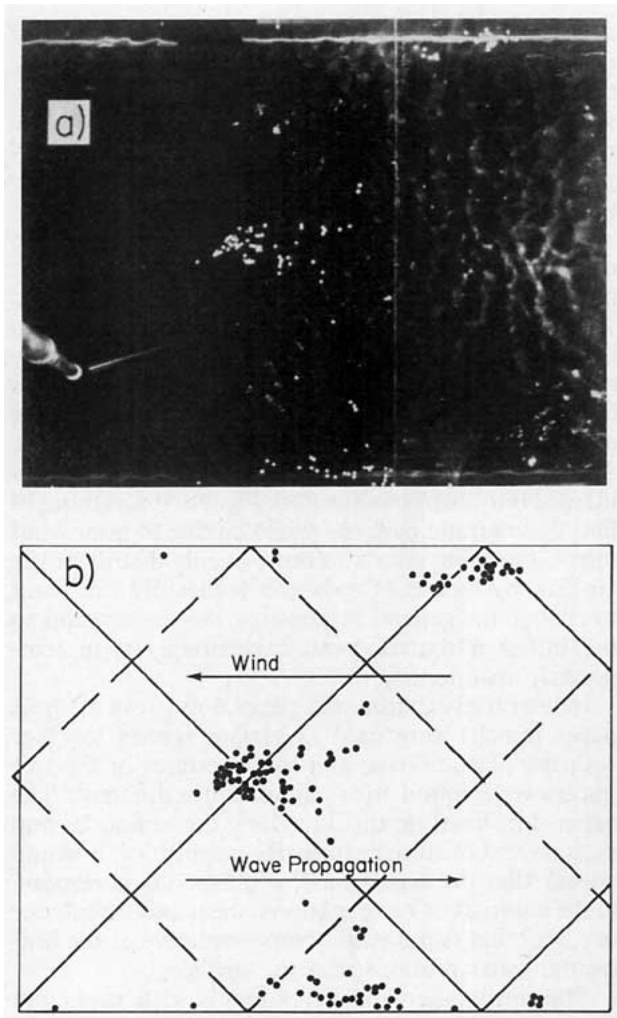

FIG. 10. (a) A photograph of the pattern of paper-dot surface tracers with both progressive crossed waves and the retrograde wind. Depth H = 16 cm, wind $\bar{w}$ = −283 cm s^{-1}. (b) The tracer pattern together with the instantaneous wave crests (solid diagonals) and troughs (dashed diagonals).

surface film, concentrating it near the wavemaker (left-hand) end of the tank.

2) A thin aluminum plate was inserted vertically into the tank through a glass cover slot near the wavemaker to keep the film at that end, and the wind was turned off for about 2 min to allow the water to come nearly to rest.

3) Paper dots were inserted through a slot at the right-hand end of the tank.

4) The aluminum plate was removed, and the wind and the wavemaker were turned on simultaneously.

5) The waves reached the tracers in about 9 s. By this time the wind had blown the tracers about 135 cm toward the waves, a surface drift speed of about 15 cm s^{-1}.

6) The photo of Fig. 10 was taken 10 s later.

Patterns of the tracers at corresponding times with and without the crossed waves were photographed for a range of wind speeds from 140 to 380 cm s^{-1} with essentially the same results. At wind speeds < 140 cm s^{-1} the surface film moved upwind (by film pressure and wave drift) too rapidly to conduct useful experiments.

A tracer asymmetry due to uneven wind is apparent in both Figs. 10 and 11. This asymmetry represents a systematic variation in the average longitudinal displacements of the tracers of about ±10%. Fig. 10 also shows about 20 cm less total wind drift to the left because of the effect of the crossed waves. A difference in the wind-generated waves is also clear, the waves being larger and more irregular in the presence of the crossed waves of Fig. 10.

5. Concluding remarks

All experiments to date are in general agreement with the CL I model of Langmuir circulations. In

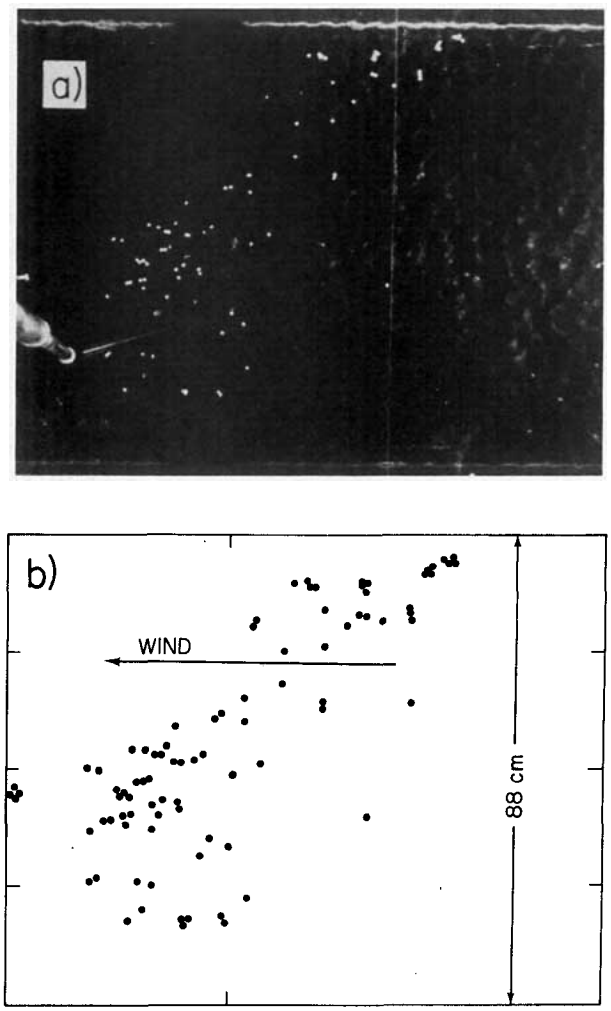

FIG. 11. An experiment identical to that of Fig. 10 but with no crossed waves.

particular, the retrograde-wind studies of Section 4 are the most convincing evidence, for they have demonstrated that a reversal of the vorticity in the wind-sheared surface layer is accompanied by a reversal of vorticity in the cells. It seems unlikely that this reversal would occur as it does if some other mechanism dominated the generation of the LC's.

The growth rate experiments of Section 3 have yielded results that cannot be directly compared with the analytical model because of various complicating experimental factors. These are primarily the wind-wave generated Langmuir circulations and the associated turbulence. The most nearly undisturbed experiment (W4) had the most rapid growth rate, however, and, following the arguments in F, this growth rate would seem to be more rapid than that predicted by theory.

The value of T for W5 seems to be rather large in relation to τ/ρ compared to the values for W4 and W7. While this may be in part due to errors in the estimates of T (especially for W7) it seems likely that the greater depth in W5 was an important factor. The greater depth would have three effects each tending to increase T. First, a larger mass of water would have to be accelerated to the equilibrium circulation. Second, energy could more easily be transferred to larger scales, in particular to one pair of cells ($\lambda_c/H = 88/39 = 2.3$) or possibly to a single cell occupying the entire tank ($\lambda_c/H = 4.5$). Large cells of this nature, often vacillating between one mode and another, are regularly observed at large t as reported in Faller (1969). Third, a shallower rigid boundary would have a larger viscous drag and would tend to reduce T.

In addition to the uncertainties in T that have already been discussed in connection with W7, two other sources of possible error, although small, do deserve mention. First, with the prograde winds, as well as with the retrograde winds, the motions of the plastic floats may be somewhat unrepresentative of the velocities of the fluid in which they are imbedded. Second, the tracer displacements are a combination of advection by the mean flow of the LC's, turbulence, and wave oscillations. In time the tracers acquire an equilibrium distribution that is a balance between the convergent effect of the mean flow, turbulent dispersion and oscillations. At that time the average v of the tracers must be zero despite the mean flow. It follows that as the tracers approach this equilibrium distribution, their average speeds must be less and less representative of the cellular motions. An analytical study of the combined effect of a convergent mean flow, turbulence and waves (Faller and Mignerey, 1982) clearly shows this effect, and further work, more directly related to the present problem, will be reported in the near future. In the present case, however, the data analysis was terminated before the tracers could become too concentrated.

Perhaps it is appropriate to note here the preliminary results of some experiments of a different sort being carried out in collaboration with Mr. Craig Perini to test the CL II mechanism of instability. In these studies small amplitude, monochromatic plane waves (on water) interact with a preexisting shear flow, O(1 s^{-1}). Having eliminated convection by careful thermal control (as indicated by the observation of dye streaks over several minutes) the shear flow alone is found to be completely stable. With waves added [amplitude O(0.1 cm), wavelength O(30 cm)], the flow breaks down into longitudinal rolls in a time, O(1 min), that is inversely related to the wave amplitude. The longitudinal rolls then interact with the shear flow and rapidly produce turbulence. Although there are some differences between these experiments and the idealized CL II theory, notably the presence of a surface film and the transient onset of waves, the results appear to be in reasonable agreement with the theoretical predictions represented in the stability diagrams of Leibovich and Paolucci (1981).

Acknowledgments. We wish to recognize the support of the National Science Foundation under Grants ATM 76-82061 and ATM 7924544, and the support in part of the Computer Science Center of the University of Maryland. This is Technical Note BN-985, Institute for Physical Science and Technology and Report No. 82-194, Department of Meteorology, University of Maryland, College Park.

APPENDIX A

The Curve-Fitting Procedure

Exponential growth curves of the form

$$\hat{V}_i = V_\infty\{1 - \exp[-(t_i - t_0)/T], \qquad \text{(A1)}$$

having the three parameters V_∞, t_0 and T and where $\hat{V}_i$ is a least-squares estimate of an observation V_i, were fitted to the observed data points with the following modification of the usual least squares procedure.

The mean-square difference between $\hat{V}_i$ and V_i is

$$\overline{\epsilon^2} \equiv \overline{(\hat{V}_i - V_i)^2} = \overline{[V_\infty(1 - E_i) - V_i]^2}, \qquad \text{(A2)}$$

where the overbar is an average over all i and where $E_i = \exp[-(t_i - t_0)/T]$. Setting $\partial\overline{\epsilon^2}/\partial V_\infty = 0$ one obtains

$$V_\infty = \frac{\overline{V_i(1 - E_i)}}{\overline{(1 - E_i)^2}}. \qquad \text{(A3)}$$

From (A2) we also find by setting $\partial\overline{\epsilon^2}/\partial t_0 = 0$ that

$$\frac{-V_\infty^2}{T}\overline{(1 - E_i)E_i} + \frac{V_\infty}{T}\overline{V_iE_i} + V_\infty\overline{(1 - E_i)^2}\frac{\partial V_\infty}{\partial t_0} - \overline{\frac{V_i}{T}(1 - E_i)}\frac{\partial V_\infty}{\partial t_0} = 0. \qquad \text{(A4)}$$

But by virtue of (A3) the sum of the last two terms in (A4) is zero so that we have simply

$$-V_\infty\overline{(1-E_i)E_i}+\overline{V_iE_i}=0. \qquad \text{(A5)}$$

Given a guess value for T and using (A3) for V_∞, (A5) is an equation of the form $f(t_0)=0$ and was solved for t_0 on an HP 41C using the prepared program SOLVE. The value of T that minimized ϵ^2 was then found by trial, and the corresponding V_∞ and t_0 were calculated.

REFERENCES

Craik, A. D. D., and S. Leibovich, 1976: A rational model for Langmuir circulations. *J. Fluid Mech.*, **73,** 401–426.

Craik, A. D. D., 1977: The generation of Langmuir circulations by an instability mechanism. *J. Fluid Mech.*, **81,** 209–223.

Faller, A. J., 1969: The generation of Langmuir circulations by the eddy pressure of surface waves. *Limnol. Oceanogr.*, **14,** 504–513.

——, 1978: Experiments with controlled Langmuir circulations. *Science*, **201,** 618–620.

——, and E. A. Caponi, 1978: Laboratory studies of wind-driven Langmuir circulations. *J. Geophys. Res.*, **83,** 3617–3633.

——, and P. Mignerey, 1982: One-dimensional turbulent dispersion in convergent and divergent flows. *Phys. Fluids*, **25,** 1306–1316.

Leibovich, S., 1977a: On the evolution of the system of wind drift currents and Langmuir circulations in the ocean. Part 1. Theory of the averaged current. *J. Fluid Mech.*, **79,** 715–743.

——, 1977b: Convective instability of stably stratified water in the ocean. *J. Fluid Mech.*, **82,** 561–581.

——, 1980: On wave-current interaction theories of Langmuir circulation. *J. Fluid Mech.*, **99,** 715–724.

——, and K. Radhakrishnan, 1977: On the evolution of the system of wind drift currents and Langmuir circulations in the ocean. Part 2. Structure of the Langmuir vortices. *J. Fluid Mech.*, **80,** 481–507.

——, and S. Paolucci, 1980a: Energy stability of the Eulerian-mean motion in the upper ocean to three-dimensional perturbations. *Phys. Fluids*, **23,** 1286–1290.

——, and ——, 1980b: The Langmuir circulation instability as a mixing mechanism in the upper ocean. *J. Phys. Oceanogr.*, **10,** 186–207.

——, and ——, 1981: The instability of the ocean to Langmuir circulations. *J. Fluid Mech.*, **102,** 141–167.

Mobley, C. D., 1977: A numerical model of wind and wave generated Langmuir circulations. Ph.D. dissertation, University of Maryland, 170 pp.

Paolucci, S., 1979: Langmuir circulations as a convective instability mechanism and its effect on the ocean mixed layer. Ph.D. thesis, Cornell University, 218 pp.

Schlichting, H., 1960: *Boundary Layer Theory*. McGraw Hill, 647 pp.

Scott, J., G. Myer, R. Stewart and E. Walther, 1969: On the mechanism of Langmuir circulations and their role in epilimnion mixing. *Limnol. Oceanogr.*, **14,** 493–503.